Applied Ocean Research 50 (2015) 155–162

Contents lists available at ScienceDirect

Applied Ocean Research

journal homepage: www.elsevier.com/locate/apor

A tool for ROV-based seabed friction measurement

S.A. Stanier[a,*], D.J. White[a], S. Chatterjee[b], P. Brunning[c], M.F. Randolph[a]

[a] Centre for Offshore Foundation Systems (COFS), University of Western Australia (UWA), Australia
[b] Indian Institute of Technology, Bombay (IIT Bombay), India
[c] Subsea 7, Singapore

ARTICLE INFO

Article history:
Received 5 June 2014
Received in revised form
16 December 2014
Accepted 25 January 2015
Available online 18 February 2015

Keywords:
Friction
Measurement
In situ
ROV
Pipeline
Mooring chain

ABSTRACT

This paper describes a new device for measuring seabed sliding resistance *in situ*, and provides an associated interpretation procedure. The device is designed to use a work class ROV as a testing platform to allow measurements to be obtained without use of a specialized geotechnical survey platform. The measurements are to assist pipeline design or analysis of the sliding resistance of other on-bottom infrastructure such as anchor chains. The device has been trialled using three tools: a flat plate, a cylindrical pipe section and a length of chain. The tools are dragged axially along the seabed using the ROV thrusters or a separate hydraulic actuator. An interpretation technique has been developed to estimate the passive resistance mobilized by the faces of the tools to eliminate end effects and to account for shape effects such as wedging. Onshore-trial tests were performed in a bed of dry sand. The individual tools exhibited different overall coefficients of friction, but the back-analysis method yielded equal interface friction angles acting on all three devices, indicating internal consistency. The interface friction angle also matched shear box test results. These outcomes confirm the correct operation of the device in drained seabed conditions, and yield useful information on the sliding resistance of pipes and chains. In addition, the back-analysis method allows measurements from one shape of tool to be used to estimate the response of other objects.

1. Introduction

Conventional offshore site investigation typically involves a combination of *in situ* penetrometer testing and sampling for laboratory testing. These penetrometer tests and sampling processes are usually conducted using a specialized vessel and drilling system. The costs of operation are high and the volume and spatial distribution of data collected are often limited.

Pipeline design requires a lengthy route to be surveyed, with accurate characterization of the surficial soil. A key design parameter is the pipe-seabed friction, which controls the tendency for progressive axial pipe movement ('walking') through cycles of operation (Bruton et al., 2008 [1]). Seabed sliding resistance or friction is also an important parameter in the design of shallow foundations and temporary clump weights used for installation operations.

There is also much uncertainty surrounding the axial sliding capacity of mooring chain resting on the seabed, as used to connect floating vessels to seabed anchors. The ISO-19901-7 [2] international standard states that "*the coefficient of friction* [between the chain and the seabed] *depends upon the nature of the seafloor and on the type of mooring line.*" In the absence of more specific data, a sliding coefficient of friction of 0.7 is given. However, this value is then qualified: "*Industry experience indicates that coefficients of friction can vary significantly for different soil conditions, and much higher values for the sliding coefficient of friction have been encountered.*"

Other standards quote different values: DNV-OS-E301 [3] quotes a chain-seabed friction coefficient of 1.0 while DNV-RP-301 [4] gives a best estimate of 0.7 and a range of 0.6–0.8. There is clearly uncertainty surrounding chain-seabed friction and *in situ* measurement of this parameter offers a solution to the dependency on the soil conditions.

This paper explores the concept of an ROV-based investigation tool for measuring seabed friction *in situ*. An ROV-based tool requires less specialized equipment compared with a conventional geotechnical survey. It is shown that the tool is able to gather repeatable and reliable data on seabed sliding resistance, which is consistent with laboratory testing using the same material.

A similar concept was described by Lambrakos [5]. In that study, a special seabed vehicle incorporating two separate pipeline segments was towed by a surface vessel. Seabed friction coefficients were back-calculated from the measured tow forces in both sand and clay soils in water depths of 9–18 m in the Gulf of Mexico. However, the system was limited to relatively shallow water locations due to the need to drag the vehicle along the seabed using a surface vessel.

* Corresponding author. Tel.: +61 447571092.
E-mail address: sam.stanier@uwa.edu.au (S.A. Stanier).

0141-1187/$ – see front matter © 2015 Elsevier Ltd. All rights reserved.
http://dx.doi.org/10.1016/j.apor.2015.01.016

Nomenclature

α	inclination angle
A	contact area
A_p	projected area
B	tool or chain link width
d	displacement
D	diameter
D_c	chain bar diameter
δ_i	interface friction angle
e	void ratio
F	force
F_h	horizontal force
$F_{p\text{-}end}$	passive force at tool end
$F_{p\text{-}int}$	internal passive force
g	gravitational acceleration
G_s	specific gravity
γ	unit weight of soil
γ_w	unit weight of water
I_D	relative density
I_R	relative dilatancy index
K_p	coefficient of passive earth pressure
m	tool mass
μ_i	interface friction coefficient
μ_t	tool friction coefficient
n	number of chain links
N	normal contact force
p'	mean stress
ϕ'	operative friction angle
Q	natural logarithm of the grain crushing strength
T	traction
τ_{ave}	average shear stress at the interface
θ	enclosed angle of circular segment
V	vertical tool-seabed reaction force
w	embedment depth
W	tool weight
$\bar{z}$	depth to centroid of area
ζ	wedging factor

A more sophisticated platform is the SMARTPIPE ([6] and [7]), which is an *in situ* testing system intended for use in deep water (down to 2500 m). A 200 mm diameter polypropylene-coated pipe section is manipulated using a three degree of freedom actuator that provides vertical, lateral and axial displacement. This tool provides detailed measurement of both pipe–soil resistance forces and also the pore pressure acting on the pipe surface. However, the hardware is highly specialized and has not found routine usage.

Remotely operated vehicles (ROVs) are routinely used offshore for support of exploration, installation and integrity monitoring work. Work class ROVs typically have a plan area of ~1 by 2 m and provide a platform from which geotechnical testing can be performed at the seabed. The wider use of ROVs as a geotechnical survey platform has long been proposed [8], and the development of ROV-based geotechnical tools has increased in recent years ([9], [10]).

This paper describes a simple apparatus for performing axial drag tests to measure seabed friction, from an ROV (see Fig. 1), using different shaped tools: a flat plate, a pipe section and a length of chain. The tool is actuated by ROV thrusters or by an electrical or hydraulic cylinder when the ROV is stationary. The drag force on the tool caused by seabed friction is measured by a load cell at the end of the tool. Trial tests of the device onshore in a test bed of dry sand have proved the concept of the device through back-calculations of the interface friction generated by each of the three tools. The tool was developed in collaboration between Subsea 7 and the University of Western Australia.

Table 1
Drag tool properties.

Tool	Property		
	Length (m)	Width (m)	Weight (N)
Plate	0.6	0.1	215.8
Pipe	0.6	0.08	255.1
Chain	0.62	0.11	127.5

2. Description of drag tool

The apparatus consists of a stainless steel frame constructed from 25 by 25 mm square hollow section (SHS). The frame measures 1 m in length, by 0.5 m wide and 0.3 m deep. This size was designed for the tool to be mounted within the standard skid of a typical work-class ROV. The corners of the frame are gusseted for rigidity and six uprights are provided for the tool suspension cables *via* 11 holes at 20 mm vertical centres (see Fig. 2).

The three tools are shown in Fig. 3 and their properties are given in Table 1. They were all made from steel and finished to the same surface roughness by sandblasting. Adjacent chain links were welded at 90° so as not to form a catenary between the suspending cables when the ROV is in flight. Stainless steel padeyes at the ends and sides of the tools connected them to the suspending cables.

Stainless steel D-shackles - attached to the suspension cables of each of the tools - are fitted through the tool padeyes, allowing adjustment of the height of the tool relative to the frame. The suspension cables are 2 mm diameter stainless steel wire cables with an ultimate breaking strain of ~2 kN. The drag force measuring cables at the ends of the tools attach to the frame *via* a pair of 3 kN pillar type load cells, which were custom-built in house at UWA and were waterproofed by being potted in urethane prior to pressure testing to 1.5 MPa.

The lengths of the suspending cables were chosen so that the weight of the tools is evenly distributed between all of the cables when the ROV is in flight with the base of the tool hanging ~150 mm below the frame. Turnbuckles on the load cell connections allow fine adjustment of the pulling cable lengths. With correct tensioning, a small tension is carried in the pulling cables when the ROV is in-flight, providing the operator with an indication of tool touchdown as the ROV is lowered to the seabed and the cables become slack.

The signals from the load cells are passed into a sealed enclosure (pressure tested to 1.5 MPa) *via* Subconn® cables and connectors. Within the sealed enclosure a DigiDAQ device [11] is used to digitize the analogue signals from the load cells. Communication to the surface vessel is achieved *via* a serial multiplexer onboard a typical work-class ROV. The DigiDAQ device was modified to output the digitized data *via* the RS232 protocol rather than the standard Ethernet interface. On the surface vessel an RS232 to Ethernet adapter (Lantronix EDS2100) converts the serial output to Ethernet, where it is logged at a PC using the standard DigiDAQ software ([11]). The data acquisition system utilizes 24 V DC power from the ROV and uses a DC–DC converter to provide the 12 V DC supply required by the DigiDAQ system.

3. Test procedure

Operation of the drag-testing device entails seven main steps:

1. The ROV is flown to the chosen test location.

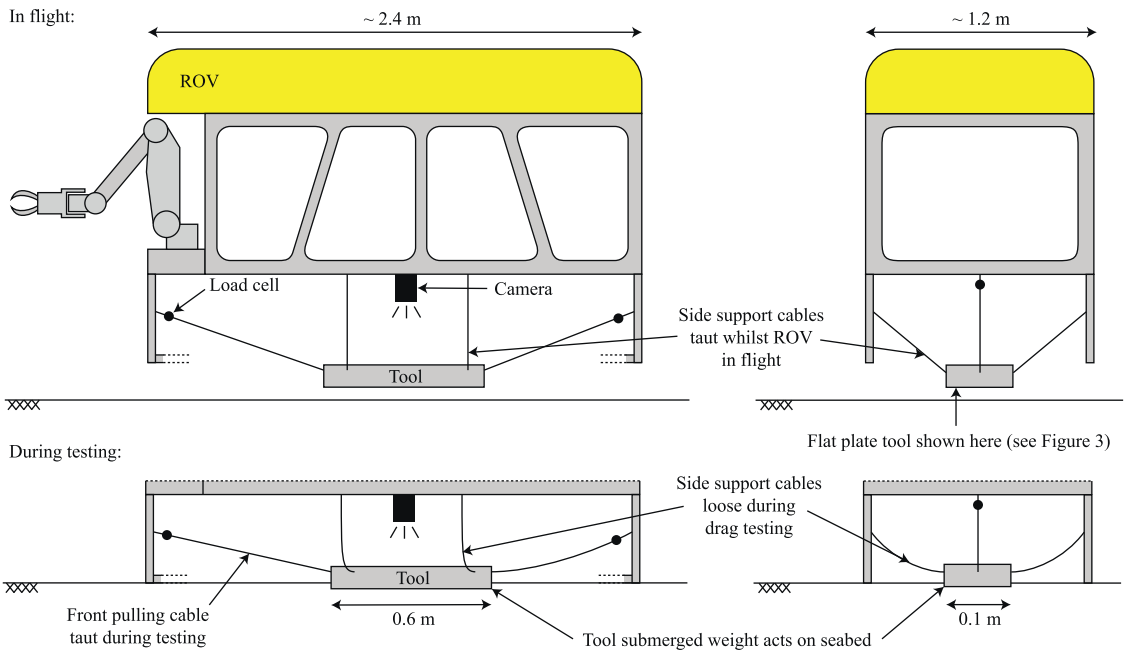

Fig. 1. Schematic of ROV-based drag test concept.

2. The ROV is lowered onto the seabed thus initiating touchdown of the tool. The load cells record a reduction in tension indicating contact with the seabed.
3. Dependent upon the expected soil behaviour at the seabed, a wait period may be allowed following touchdown for consolidation of the soil beneath the tool.
4. Following the wait period, the tool is dragged axially over the seabed. This is achieved either using the axial thrusters and movement of the ROV, or by displacing the tool frame *via* a hydraulic or electrical actuator.
5. The direction of movement is reversed and a further drag test is performed. For this reversal event, the drag force is measured by the alternate load cell at the other end of the tool. Further cycles are performed if required.
6. The ROV and tool is then lifted clear of the seabed.
7. The ROV is then flown to another test location before repeating the test sequence.

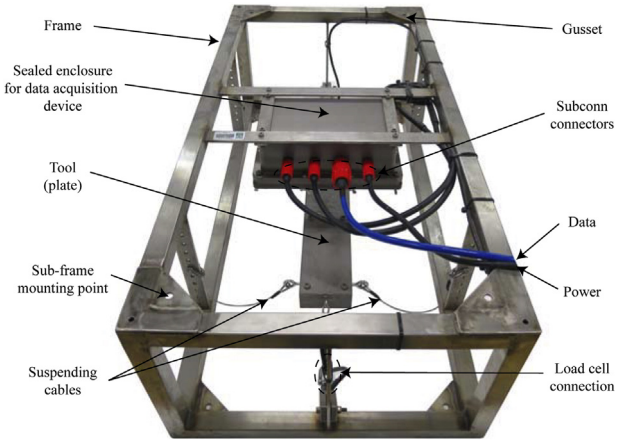

Fig. 2. ROV mounted device and its major features.

4. Initial testing programme

Initial onshore testing of the device was performed to confirm the satisfactory performance of the equipment and to determine a suitable interpretation method that provides consistent seabed interface friction parameters across the different tool types.

The onshore testing was performed in a 2 by 2 m test pit filled to a depth of ~0.3 m with dry silica sand with the properties given in Table 2. The sand pit was prepared with a flat surface and the drag-testing frame was dragged over the test pit on rails. Cycles of forward and reverse movement over 1 m length were then performed. The displacement rate was ~0.05 m/s. Tests were performed using each tool: plate, pipe and chain.

Fig. 3. Array of drag tools including (a) plate, (b) pipe and (c) chain sections along with suspending cables and D-shackles.

Table 2
Properties of silica sand used for testing.

Critical angle of friction, ϕ_{cv} (°)	33
Specific gravity, G_s (−)	2.65
Minimum voids ratio, e_{min} (−)	0.45
Maximum voids ratio, e_{max} (−)	0.75
Unit weight, γ (kN/m^3) (I_D = 0.5)	16.3

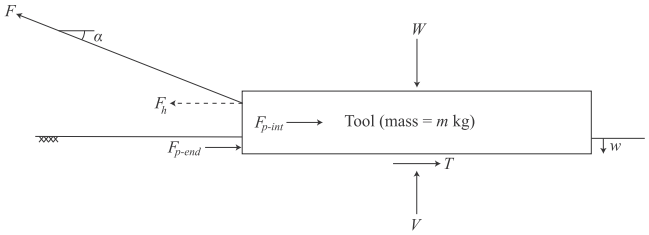

Fig. 4. Free body diagram of tool during testing.

5. Back-analysis of measured drag force

As illustrated in Fig. 1, the pulling cables are inclined during the drag event so the measured load must be converted for forces parallel and perpendicular to the seabed (Fig. 4). For this onshore testing (in air, rather than water), the tool weight, W, is:

$$W = mg \tag{1}$$

where g is gravitational acceleration (9.81 m/s^2) and m is the mass of the tool. From vertical equilibrium, the vertical tool-seabed reaction force, V, is:

$$V = W - F\sin\alpha \tag{2}$$

where F is the measured force from the load cell on the pulling cable and α is the inclination of the drag cable from the horizontal. For non-planar contact with the seabed (*i.e.* the pipe and chain) the integral of the normal stresses over the contact surface area is greater than the weight of the tool. This is due to a wedging effect provided by the horizontal components of the normal contact stresses over the non-planar surfaces of the tool [12]. The normal contact force between the tool and the seabed, N, exceeds V by a wedging factor ζ:

$$N = \zeta V \tag{3}$$

After [12], ζ was taken as:

$$\zeta = \frac{2\sin\theta}{\theta + \sin\theta\cos\theta} \tag{4}$$

where θ is the enclosed angle of the circular segment of the pipe or chain that is embedded:

$$\theta = \cos^{-1}\left(1 - \frac{2w}{D}\right) \tag{5}$$

where w is the embedment depth and D is the diameter of either the pipe or chain bar section.

The horizontal component of the measured force F_h, is equivalent to the drag force minus the passive force generated at the leading end of the tool F_{p-end}, (illustrated in 4):

$$F_h = F\cos\alpha - F_{p-end} \tag{6}$$

The traction generated between the surface of the tool and the seabed T, is given by:

$$T = \tau_{ave}A = F_h - F_{p-\mathrm{int}} \tag{7}$$

where τ_{ave} is the average shear stress at the interface, A is the contact area and F_{p-int} is the internal passive force generated by the passive resistance of soil within the tool, such as generated between the links of a chain during axial sliding.

There is no end effect force F_{p-end}, for the chain (since each link in contact with the seabed will generate passive resistance it is not considered an end effect), while for the plate and pipe it is estimated as:

$$F_{p-end} = \gamma\bar{z}K_pA_p \tag{8}$$

Conversely, no internal passive force F_{p-int}, is generated by the plate and pipe sections as these tools simply slide along the seabed, while for the chain section it is estimated as:

$$F_{p-\mathrm{int}} = n\gamma\bar{z}K_pA_p \tag{9}$$

where $\bar{z}$ is the depth of the centroid of the projected area below the soil surface, γ is the unit weight of the soil (to be replaced by the effective unit weight for offshore testing), K_p is the coefficient of passive earth pressure, A_p is the projected frontal surface area subjected to passive resistance and n is the number of chain links. This assumes that for the chain the internal passive force, F_{p-int}, is generated by the sum of the passive resistance acting over the projected frontal area of each chain link.

The unit weight of the dry soil is:

$$\gamma = \frac{G_s\gamma_w}{1+e} \tag{10}$$

where G_s is the specific gravity and e is the voids ratio.

For the plate (Fig. 5a), $\bar{z}$ and A_p are given by:

$$\bar{z} = \frac{w}{2} \tag{11}$$

$$A_p = wB \tag{12}$$

where w is the embedment depth and B is the width of the tool.

For the pipe (Fig. 5b), $\bar{z}$ and A_p are given by:

$$\bar{z} = \frac{2D\sin^3\theta}{3\left(2\theta - \sin 2\theta\right)} - \left(\frac{D}{2} - w\right) \tag{13}$$

$$A_p = \frac{D^2}{8}\left(2\theta - \sin\left(2\theta\right)\right) \tag{14}$$

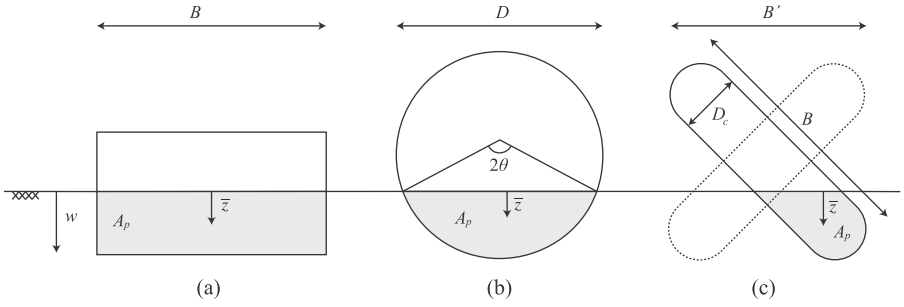

Fig. 5. Schematic of projected areas mobilizing passive resistance during sliding: (a) plate, (b) pipe and (c) chain.

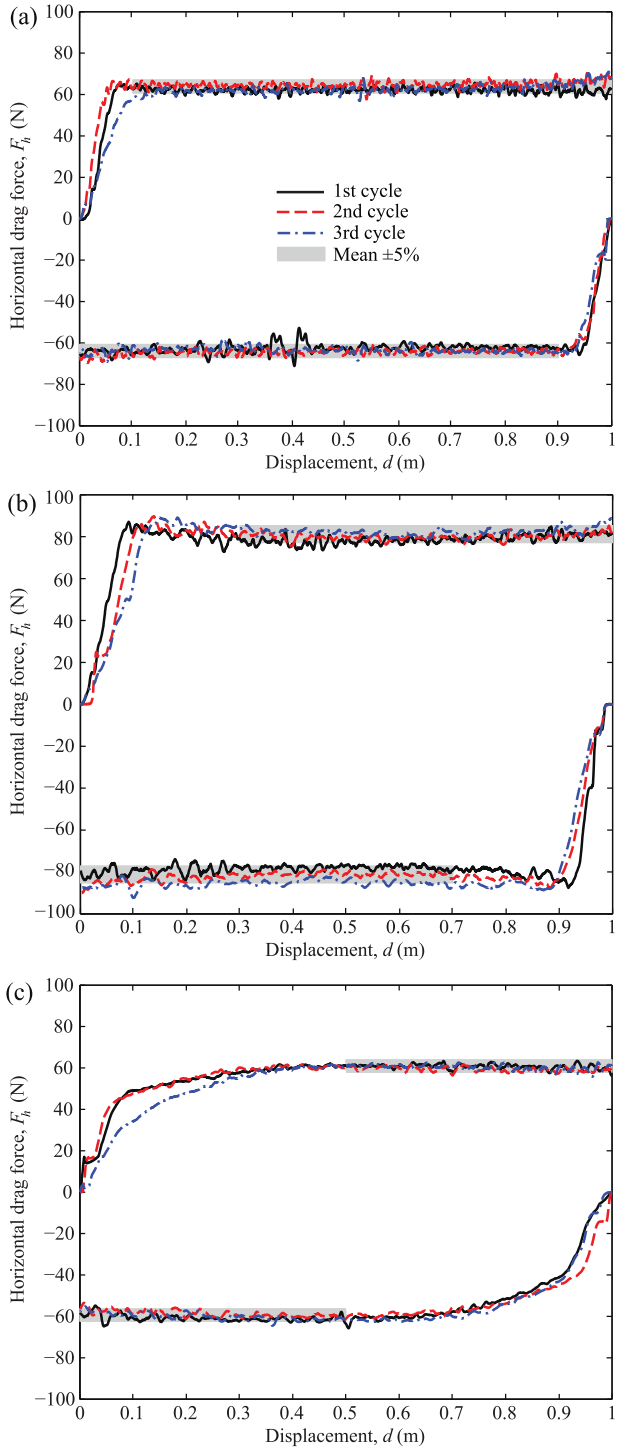

Fig. 6. Repeatability of drag force responses: (a) plate, (b) pipe and (c) chain.

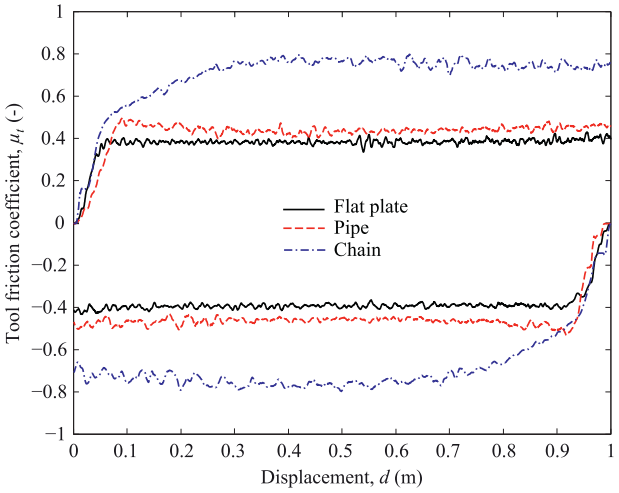

Fig. 7. Comparison of tool friction coefficient, μ_t, for each tool.

where θ is as given by equation 5 and illustrated in Fig. 5.

Calculation of $\bar{z}$ and A_p for the chain is more complicated due to the complex geometry (Fig. 5c). Passive resistance is mobilized on both the front link and also internally on the projected frontal area of each of the links along the chain. For simplicity, $\bar{z}$ is approximated as half of the embedment depth:

$$\bar{z} \approx \frac{w}{2} \tag{15}$$

Similarly, A_p is an approximation of the frontal area presented by each chain link, which is proportional to the embedment depth:

$$A_p = \frac{w\left(BD_c - D_c^2 + \frac{\pi D_c^2}{4}\right)}{\left(D_c + \sqrt{\frac{(B-D_c)^2}{2}}\right)} \tag{16}$$

where D_c is the chain-bar diameter and B is the chain-link width. The numerator is equivalent to the frontal projected area of the chain link multiplied by the embedment depth, w, as illustrated in Fig. 5. The denominator is the total height of the inclined link in the vertical plane; hence, A_p is taken as proportional to an approximation of the normalized embedment depth. Some embedded projected areas within the links themselves have been ignored for simplicity, whilst no correction has been made for the rounded corners of the links and the subsequent reduced passive earth pressures that may be generated on these curved surfaces. These two simplifications tend to offset each other. The result is a simple calculation for passive resistance within a chain and is shown later to be adequate.

For all three tools the coefficient of passive earth pressure is taken as:

$$K_p = \frac{1+\sin\phi'}{1-\sin\phi'} \tag{17}$$

To account for stress-dependent dilatancy, the operative angle of friction ϕ', is estimated using correlations from Bolton [13]:

$$\phi' = 3I_R + \phi_{cv} \tag{18}$$

where ϕ_{cv} is the constant volume friction angle and I_R is a relative dilatancy index and is taken as:

$$I_R = I_D\left(Q - \ln p'\right) - 1 \tag{19}$$

where I_D is the relative density of the sand, Q is the natural logarithm of the grain crushing strength and p' is the mean stress, estimated here as:

$$p' = \bar{z}\gamma\left(\frac{1+2K_p}{3}\right) \tag{20}$$

Alternative estimates for the mean stress at failure were considered. One alternative is to take an estimate of p' that is broadly representative of plane strain–stress conditions:

$$p' = \bar{z}\gamma\left(\frac{1+K_p}{2}\right) \tag{21}$$

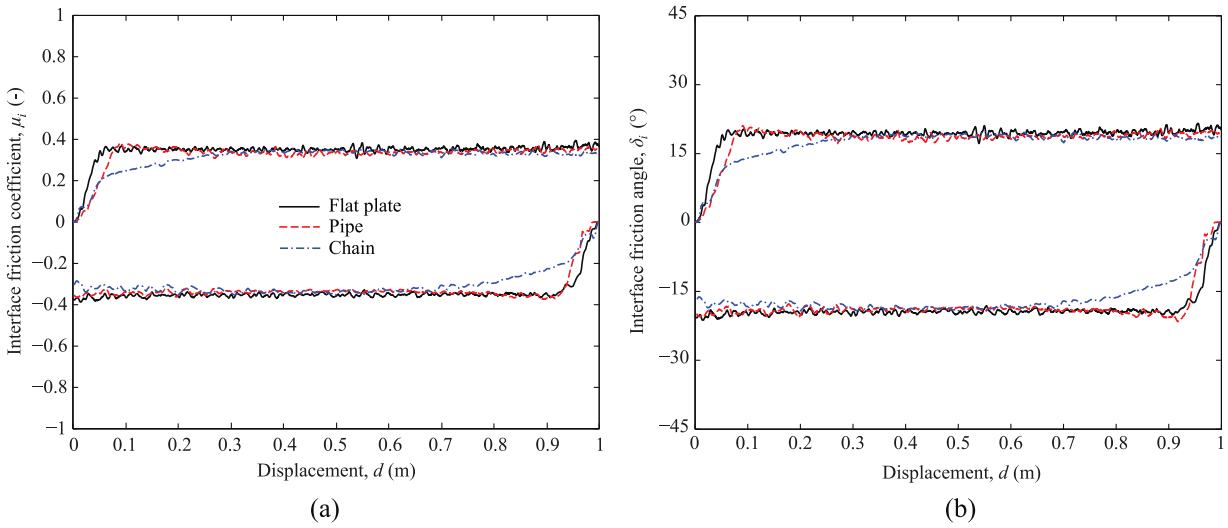

Fig. 8. Comparison of (a) interface friction coefficient, μ_i, and (b) interface friction angle, δ_i, for each tool.

Another alternative estimation adopted in pile engineering is to approximate the average mean stress at failure as equivalent to the geometric mean of the *in situ* vertical stress and the end bearing pressure at the pile tip [14]. For this problem, an equivalent method would result in the mean stress being taken as the geometric mean of the *in situ* vertical stress and the passive resistance generated in the failure zone ahead of the tool, whereby:

$$p' = \bar{z}\gamma\sqrt{K_p} \tag{22}$$

The adoption of either of these alternative approximations was found to have a negligible effect on the results of the proposed back-analysis. Due to the relatively small aspect ratio of the width of the tool, with respect to its length, it was deemed that the pseudo-triaxial approximation of equation 20 was most appropriate for this back-analysis.

Bolton [13] found that limiting the relative dilatancy index to a range of $0 \leq I_R \leq 4$ provided a good correlation to experimental measurements, effectively capping the operative friction angle at very low confining stresses. It was uncertain at the time what the effect of extremely low stress levels (resulting in high I_R) might be on the mechanical response of sands. However, Fannin [15] later published data indicating that at extremely low stress levels (<5 kPa) the operative friction angle continues to rise due to stress dilatancy, so no such limit has been applied here.

The tool friction coefficient μ_t, which accounts for the end effects but not wedging, is equal to:

$$\mu_t = \frac{F_h}{V} = \tan\delta_i \tag{23}$$

Alternatively, the interface friction coefficient, μ_i, is corrected for wedging effects and the passive forces caused by both the end effects and the internal passive resistance of the soil between the chain links. It is, therefore, a property of the soil-tool interface (not the tool shape) and is defined as:

$$\mu_i = \frac{T}{N} = \tan\delta_i \tag{24}$$

6. Results of drag tests

A series of cyclic drag tests was performed with each tool. The pulling cable and tool inclination angles were measured at the end of each sweep while the embedment, w, of the tool at the leading edge was also recorded for later back-analysis of the passive resistance effects.

Figure 6 presents the first three cycles of the drag tests for each of the tools after correction for the inclination of the pulling cable α, which was measured at the end of each axial sweep. For this series of experiments, α was typically in the range of 25–30°, with the inclination angle increasing proportionally with the embedment of the tool. Due to the pulling cable inclination each of the tools tended to rise slightly at the leading edge during each sweep causing the tool to become inclined. The tool inclination was also measured at the end of each axial sweep and was found to be minimal for the plate and pipe (<1°) and moderately higher for the significantly lighter chain (~2.5°). The initial mobilization distance required to achieve a steady state was $\delta \sim 0.1$ m for the plate and the pipe and $\delta \sim 0.5$ m for the chain. The difference reflects the progressive build-up of passive resistance. The chain initially pitched slightly before returning to a near-horizontal state and took a greater displacement before a steady pattern of sand flow around the links was created. The mean drag force beyond the initial mobilization is highlighted by a band representing a + -5% range about this mean. The traces in each test remain within this band, showing excellent steadiness and cyclic repeatability of the drag force.

Normalized measures of drag force were derived using the back-analysis method outlined previously. The steady state embedment measured during testing was used in the calculation of the passive forces, F_{p-end} and F_{p-int} ($w \sim 0.04$ m, $w \sim 0.02$ m and $w \sim 0.045$ m for the plate, pipe and chain, respectively) whilst the relative density was estimated to be 0.5.

The simplest normalized measure of drag force is the tool friction factor, μ_t, which accounts for the passive force due to end effects and is presented in Fig. 7. Due to the small frontal areas and embedment depths, passive end effects accounted for only ~10 and 1% of the total horizontal drag force, F_h, for the plate and pipe sections respectively. The plate gave the lowest friction factor of $\mu_t \sim 0.4$, while the pipe friction factor was marginally higher at $\mu_t \sim 0.45$ due to wedging. In contrast, the chain friction is significantly higher ($\mu_t \sim 0.75$) due to a combination of wedging effects and the mobilization of significant passive resistance on the projected frontal areas of each of the links within the chain.

To eliminate the internal passive resistance and wedging effects, Fig. 8 (a) and (b) present the interface friction factor, μ_i, and the interface friction angle, δ_i, for the three tools following the method outlined previously. At these embedment depths, the wedging correction factor, ζ, was ~1.17 for the pipe and a maxima of 1.27 for the chain (since the chain was always embedded to a depth greater than the bar diameter during steady sliding). The internal passive

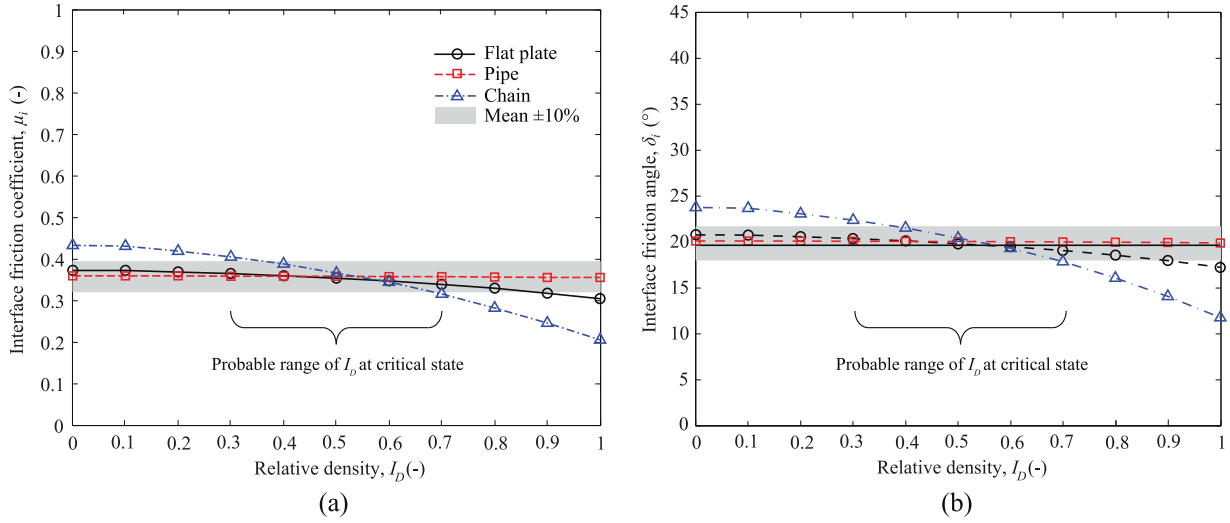

Fig. 9. Sensitivity of (a) interface friction coefficient, μ_i, and (b) interface friction angle, δ_i, to relative density, I_D.

effect for the chain is far more significant than the passive end effect for the plate or pipe, accounting for ~30% of the total horizontal drag force, F_h. For this interpretation, all three tools yield a similar interface friction factor of ~0.35 and an interface friction angle of ~20°. The back-analysis method,therefore, appears to capture the passive resistance and wedging effects accurately.

The impact of relative density on the friction parameters derived is illustrated in Fig. 9. From a relatively loose ($I_D \sim 0.3$) to a relatively dense ($I_D \sim 0.7$) initial state the back-calculated friction parameters for all tools only vary by approximately ±10%, indicating that the back-analysis method proposed is largely insensitive to the relative density of the soil.

This outcome is very valuable. It provides a basis on which measurements from a single drag tool–such as the simple plate–can be converted to equivalent friction factors for pipes or chains, using the passive resistance and wedging factor adjustments described earlier. The simple plate has the benefit of being easier to fabricate and deploy, compared to the pipe and chain. The weight is easily adjustable by adding additional sub-plates.

7. Comparison with laboratory tests

To further validate the outcomes from the trial tests, a series of interface shear-box tests were performed at comparable stress levels to those applied by the drag tools (~5 kPa). A steel interface prepared to the same roughness finish as the tools was used as the interface in the lower half of a 100 by 100 mm direct shear box. A total of five tests were performed on the test sand: three under normal stresses of 5.7 kPa and one each with normal stresses of 4.8 and 6.6 kPa. To minimize the friction between the two halves of the shear box, a Polytetraflouroethylene (PTFE) box was used. Any remaining friction was corrected for following the procedure proposed by Lehane and Liu [16]. For each test, the sand was poured into an 80 mm diameter section cut through the upper half of the PTFE shear box before being lightly tamped flat with the loading cap giving initial relative densities in the range of 0.4–0.5.

The five corrected responses are presented in Fig. 10, in terms of the measured interface friction coefficient, μ_i, and interface friction angle, δ_i, ignoring any initial peak in resistance. Average values were $\mu_i = 0.39$ and $\delta_i = 21°$, which are within 10% of the drag tool measurements. The fluctuation in the shear box data was ±10%. This is greater than the noise on the drag tool measurements, perhaps due to the smaller surface area on which the interface friction is measured in the shear box tests (approximately ~0.005 m^2 compared to ~0.06 m^2 for the drag tools). One benefit of the drag tool is the large area over which the interface friction is measured. This comparison indicates that the new device offers an accurate *in situ* method for assessing drained seabed friction properties.

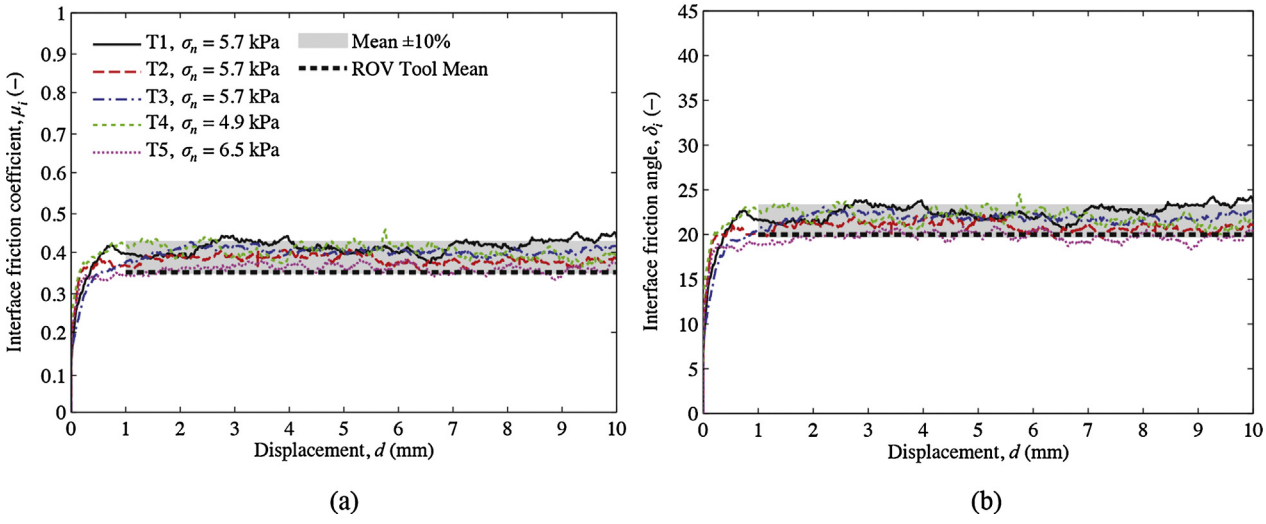

Fig. 10. Comparison of interface shear box and drag tool results: (a) interface friction coefficient, μ_i, (b) interface friction angle, δ_i.

8. Conclusions

A new tool has been devised for the *in situ* measurement of seabed friction properties using an ROV as a mobile testing platform. A simple interpretation method is provided to account for wedging and end effects. The device is designed for marine use, and is compatible with the power and data systems of typical work-class ROV. Trial testing is reported from an onshore test bed of dry sand. The results have been compared to conventional laboratory testing of interface friction properties on the same material. The following conclusions have been reached:

- Drained sliding resistance, or seabed friction, can be measured reliably and repeatably using the device with minimal measurement noise. Various tool shapes have been trialled including a flat plate, a pipe section and a length of chain, all fabricated from steel.
- The results are interpreted to account for end effects and wedging, making measurements from all three tools shapes directly comparable in terms of the steel–soil interface friction coefficient. The interpretation accounts for stress-dependent dilatancy effects but is relatively insensitive to the initial state of the soil (*i.e.* relative density).
- The steel–soil interface friction coefficient measured using the tool agreed to be within 10% with results from conventional interface shear box tests.
- The chain-seabed friction coefficient was ~0.75, which is more than double the steel–soil interface friction coefficient (~0.35) due to the influence of the passive resistance presented by the frontal area of the chain links.
- The reliable interpretation method allows the sliding resistance of different objects, such as a pipeline or chain, to be inferred from the response of a simple flat plate. This potentially precludes the need for testing with multiple shapes of tool as the response of one can be inferred from another.

Acknowledgements

The work forms part of the activities of the Centre for Offshore Foundation Systems (COFS), at the University of Western Australia, which is supported by the Lloyd's Register Foundation as a Centre of Excellence and is a node of the Australian Research Council (ARC) Centre of Excellence in Geotechnical Science and Engineering. The second author is supported by an ARC Future Fellowship and holds the Shell Energy and Minerals Institute (EMI) Chair in Offshore Engineering. The financial support of Subsea 7 in the development of the device described is gratefully acknowledged.

References

[1] Bruton D, White DJ, Carr M, Cheuk CY. Pipe-soil interaction with flowlines during lateral buckling and pipeline walking. In: The SAFEBUCK JIP. Offshore Technology Conference. 2008. Paper OTC 19589.
[2] ISO-19901-7. Petroleum and natural gas industries – specific requirements for offshore structures – Part 7: Station keeping systems for floating offshore structures and mobile offshore units. Geneva, Switzerland: International Organization for Standardization; 2005.
[3] DNV-OS-E301. Position mooring – recommended practice. Oslo, Norway: Det Norske Veritas; 2013.
[4] DNV-RP-E301. Design and installation of fluke anchors – recommended practice. Oslo, Norway: Det Norske Veritas; 2012.
[5] Lambrakos KF. Marine pipeline soil friction coefficients from in-situ testing. Ocean Eng 1985;12(2):131–50.
[6] Hill AJ, Jacob H. In-situ measurement of pipe-soil interaction in deep water. In: Proc. Offshore Technology Conference. 2008. Paper OTC 19528.
[7] White DJ, Hill AJ, Westgate ZJ, Ballard J-C. Observations of pipe-soil response from the first deep water deployment of the SMARTPIPE. In: International Symposium for Frontiers in Offshore Geotechnics II. 2010. p. 851–6.
[8] Geise JM, Kolk HJ. The use of submersibles for geotechnical investigations. In: Proceedings of Submarine Technology, Paper 7.3. 1983.
[9] Newson TA, Bransby MF, Brunning P, Morrow DR. Determination of undrained shear strength parameters for buried pipeline stability in deltaic soft clays. In: Proceedings of the 14th International Offshore and Polar Engineering Conference (ISOPE 2004), vol. 2. 2004. p. 38–433.
[10] Geomarine, Datasheet available at: http://www.geomarine.co.uk/downloads/Datasheet_geoROV1.pdf Geotechnical Equipment: geoROV Seabed CPT and Sampling System; 2014.
[11] Gaudin C, White DJ, Boylan NP, Breen J, Brown T, De Catania S, et al. A wireless high speed data acquisition system for geotechnical centrifuge testing. Meas Sci Technol 2009;20:11. Paper 095709.
[12] White DJ, Randolph MF. Seabed characterization and models for pipeline–soil interaction. Int J Offshore Polar Eng 2007;17(3):193–204.
[13] Bolton MD. The strength and dilatancy of sands. Géotechnique 1986;36(1):65–78.
[14] Randolph MF, Jamiolkowski MB, Zdravkovic L. Load carrying capacity of foundations. In: Skempton Memorial Conference– Advances in geotechnical engineering. 2004. p. 207–40.
[15] Fannin RJ, Eliadorani A, Wilkinson JMT. Shear strength of cohesionless soils at low stress. Géotechnique 2005;55(6):467–78.
[16] Lehane BM, Liu QB. Measurement of shearing characteristics of granular materials at low stress levels in a shear box. Geotechn Geol Eng 2013;31(1):329–36.